

Realization of Practical Eightfold Fermions and Fourfold van Hove Singularity in TaCo₂Te₂

Hongtao Rong^{1*}, Zhenqiao Huang^{1,7*}, Xin Zhang^{2,8*}, Shiv Kumar^{3*}, Fayuang Zhang¹, Chengcheng Zhang¹, Yuan Wang¹, Zhanyang Hao¹, Yongqing Cai¹, Le Wang¹, Cai Liu¹, Xiao-Ming Ma¹, Shu Guo¹, Bing Shen⁴, Yi Liu⁵, Shengtao Cui⁵, Kenya Shimada³, Quansheng Wu^{6,10}, Junhao Lin¹, Yugui Yao^{2,8}, Zhiwei Wang^{2,8,9#}, Hu Xu^{1#}, and Chaoyu Chen^{1#}

¹ Shenzhen Institute for Quantum Science and Engineering (SIQSE) and Department of Physics, Southern University of Science and Technology (SUSTech), Shenzhen 518055, China.

² Centre for Quantum Physics, Key Laboratory of Advanced Optoelectronic Quantum Architecture and Measurement, School of Physics, Beijing Institute of Technology, Beijing 100081, China.

³ Hiroshima Synchrotron Radiation Centre, Hiroshima University, Higashi-Hiroshima, Hiroshima 739-0046, Japan.

⁴ School of Physics, Sun Yat-Sen University, Guangzhou 510275, China.

⁵ National Synchrotron Radiation Laboratory, University of Science and Technology of China, Hefei, Anhui 230029, China.

⁶ Beijing National Laboratory for Condensed Matter Physics, and Institute of Physics, Chinese Academy of Sciences, Beijing 100190, China.

⁷ Department of Physics, The Hong Kong University of Science and Technology, Clear Water Bay, Hong Kong, China.

⁸ Beijing Key Lab of Nanophotonics and Ultrafine Optoelectronic Systems, Beijing Institute of Technology, Beijing 100081, China.

⁹ Material Science Center, Yangtze Delta Region Academy of Beijing Institute of Technology, Jiaxing 314011, China.

¹⁰ University of Chinese Academy of Sciences, Beijing 100049, China.

* These authors contributed equally to this work.

#Correspondence should be addressed to Z.W. (zhiweiwang@bit.edu.cn), H.X. (xuh@sustech.edu.cn) and C.C. (cheny@ustech.edu.cn)

Space groups describing the symmetry of lattice structure allow the emergence of fermionic quasiparticles with various degeneracy in the band structure. Theoretical efforts have predicted many materials hosting fermions with the highest degeneracy, *i.e.*, eightfold fermions, yet lacking experimental realization. Here, we explore the band degeneracies in TaCo_2Te_2 crystals. Through systematic experimental and theoretical analyses, we establish TaCo_2Te_2 as a nonsymmorphic crystal with negligible spin-orbit coupling (SOC) and long-range magnetic order. These critical properties guarantee the first realization of practical eightfold fermions and fourfold van Hove singularity, as directly observed by photoemission spectroscopy. TaCo_2Te_2 serves as a topological quantum critical platform, which can be tuned into various magnetic, topologically trivial, and nontrivial phases by adding strain, magnetic field, or SOC. The latter is demonstrated by our first-principles calculations, which show that enhancing SOC in TaCo_2Te_2 will promote the experimental observation of bulk hourglass fermions. Our results establish TaCo_2Te_2 as a unique platform to explore states of matter intertwining magnetism, correlation, symmetry, and band topology.

It has been an eternal theme in condensed matter physics to explore emerging low-energy elementary excitations from many-body interactions and/or symmetry constraints. In analog to high-energy physics where the Pioncaré symmetry allows relativistic massless Weyl and Dirac fermions, in condensed matter physics Weyl and Dirac type low-energy quasiparticle excitations have been realized based on materials like graphene [1,2], topological insulator [3-6] and topological semimetals [7-14]. At zero momentum, Weyl and Dirac fermions are twofold and fourfold degenerate, respectively. Moreover, as subgroups of the Pioncaré symmetry, the 230 space groups in condensed matter physics impose fewer constraints on the allowed types of fermions. New fermionic quasiparticles beyond high-energy physics, including threefold, sixfold, and eightfold fermions, can emerge as band degeneracy [15-26]. Experimental exploration of such band degeneracy represents a major and yet-to-be accomplished task.

Table I: Experimental observation of different types of fermions in material families.

| order of dispersion n | band degeneracy g | | | | |
|-------------------------|---|-------------|---|-----------------------------|--|
| | 2 | 3 | 4 | 6 | 8 |
| 1 | TaAs [7-11], MoTe ₂ [27-29], LaAlGe [30], TaIrTe ₄ [31], YbMnBi ₂ [32], Co ₂ MnGa [33], Co ₃ Sn ₂ S ₂ [34] | MoP [35,36] | Na ₃ Bi [13,14] Cd ₃ As ₂ [12] PtSe ₂ [37-42] | CoSi [43-47] PdBiSe [48] | TaCo ₂ Te ₂ This work |
| 2 | ? (awaiting experimental proof) | ? | α -Sn [49] | PdSb ₂ [50-52] | Forbidden |
| 3 | ? | Forbidden | ? | Forbidden | Forbidden |

In Table I, the spectroscopic observation of fermionic excitations as band degeneracy in crystalline materials is summarized according to the band degeneracy \mathbf{g} and the order of dispersion \mathbf{n} . According to theoretical analysis, there exist cubic ($\mathbf{n} = 3$) Weyl and Dirac fermions [22,24] yet lacking experimental observation. Quadratic ($\mathbf{n} = 2$) Dirac and sixfold fermions have been observed directly by angle-resolved photoemission spectraoscopy (ARPES) in α -Sn [49] and PdSb₂ [50-52], respectively. Besides that, all the experimentally realized fermionic quasiparticles are of linear dispersion ($\mathbf{n} = 1$) with band degeneracy $\mathbf{g} = 2, 3, 4, 6$. However, for quasiparticles with the highest band degeneracy, *i.e.*, eightfold fermions, despite its theoretical prediction based on space groups 130, 135, 218, 220, 222, 223, 230 [16,20,22,25,26], the spectroscopic observation is still missing. This is particularly due to the difficulty in growing or handling the candidate materials [53-55]. Our approach to overcome this is to seek materials with negligible spin-orbit coupling (SOC) effect, which looses symmetry constraints and expands the space group selection.

In this work, we report the practical realization of eightfold fermion in a nonsymmorphic (space group 62) crystal TaCo₂Te₂. Magnetic property measurements reveal no signature of long-range magnetic order despite the existence of Co atoms. ARPES measurement revealed a double Dirac cone (DDC) feature at the Brillouin zone (BZ) \bar{X} point. Density functional theory (DFT) analysis prove this feature as an eightfold degenerate node at the S point of bulk BZ, protected by the combination of crystalline and time-reversal symmetry. Inclusion of SOC only opens a negligible gap, rendering a practical realization of eightfold fermions. Such symmetry combination also protects a fourfold (robust against SOC) van Hove singularity (VHS) at Z close to the Fermi level (E_F), which represents a new type of VHS beyond the recent classifications of high-order VHSs [56,57]. Both the eightfold fermion and fourfold VHS have been directly observed by ARPES. These magnetic and electronic properties establish TaCo₂Te₂ as a topological quantum critical platform that can be tuned into various magnetic, topologically trivial, or nontrivial phases [16,20], say, by inducing magnetism, SOC, symmetry breaking via chemical, strain, or band engineering. As an example, we use DFT calculation to prove that enhancement of SOC would promote practical ARPES observation of bulk hourglass fermions for the first time. These results suggest TaCo₂Te₂ as a unique platform to explore emergent physics intertwining magnetism, correlation, symmetry, and band topology.

TaCo₂Te₂ crystallizes in an orthorhombic structure [58]. Using single-crystal X-ray diffraction (SCXRD) we determine its lattice structure as lattice constants $a = 6.6116 \text{ \AA}$, $b = 6.5735 \text{ \AA}$, $c = 17.783 \text{ \AA}$ in space group 62 (*Pmcn*). The corresponding BZ is shown in Fig. 1(b). The crystallinity of as-grown single crystals was examined by XRD. As shown in Fig. 1(c), all the diffraction peaks can be well indexed by the (00l) reflections with $c = 17.783 \text{ \AA}$. The magnetic

property of TaCo_2Te_2 is shown in Fig. 1(d). First, no order behaviour can be observed from $\chi - T$ measurement, indicating the absence of magnetic order in the current temperature region. Between 100 K and 300 K, the slope of $\chi - T$ curves can be positive or negative depending on samples, neither of which can be fitted by Curie-Weiss law, indicating extrinsic origin. Secondly, the value of χ in TaCo_2Te_2 is 3 orders of magnitude lower compared to typical cobalt compound $\text{Co}_3\text{Sn}_2\text{S}_2$ [59,60], suggesting negligible Co moment. Thirdly, the field-dependent magnetization ($M - H$) curves also show no signature of saturation or hysteresis. All the above magnetic properties enable us to omit the magnetism of TaCo_2Te_2 in the following electronic structure study.

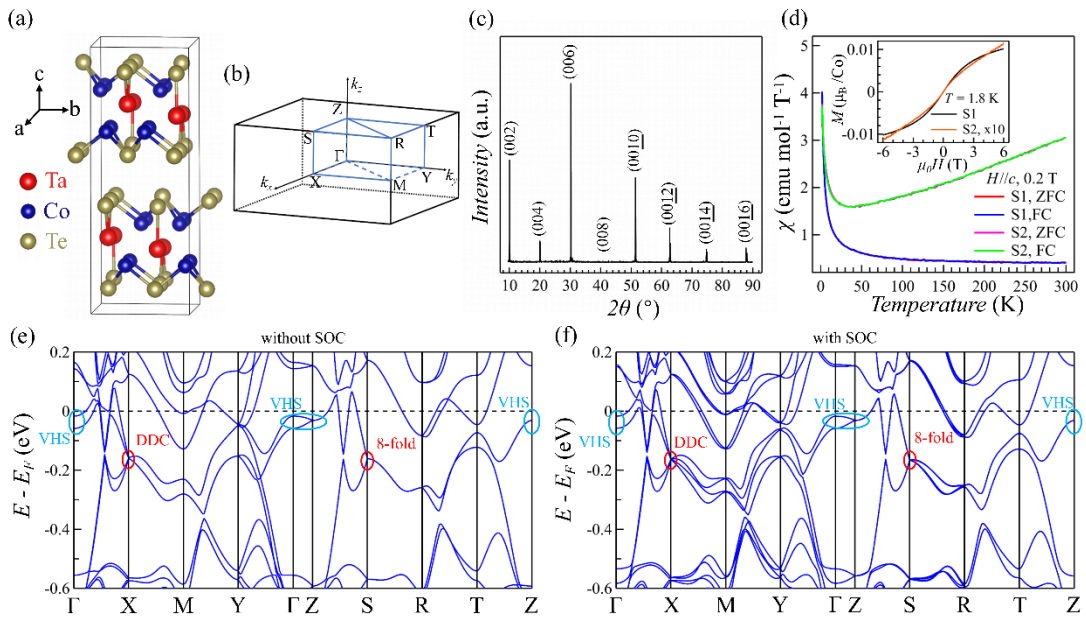


FIG. 1. Eightfold fermions and fourfold VHS in nonsymmorphic TaCo_2Te_2 with negligible magnetic order. (a) Crystal structure of TaCo_2Te_2 . (b) Three-dimensional BZ of TaCo_2Te_2 . (c) Single crystal x-ray diffraction (XRD) result taken at 300 K. (d) Zero-field-cooled (ZFC) and field-cooled (FC) magnetic susceptibility (χ) vs temperature (T) for magnetic field $H = 0.2 \text{ T}$ parallel to the c axis. Inset: Field-dependent magnetization (M) at 1.8 K. (e, f) DFT calculated dispersions along the high-symmetry path without considering SOC (e) and with SOC (f).

Figures 1(e) and 1(f) show the band structure of TaCo_2Te_2 along the high-symmetry path calculated by DFT without and with considering SOC, respectively. Two exotic features in the $k_z = 0$ plane ($\Gamma - X - M - Y - \Gamma$ plane) are noticeable. The first one is a DDC feature ($\sim -0.17 \text{ eV}$) at X point (highlighted by red ellipses). Fig. 2(g) shows that this DDC has two fourfold degenerate points separated by a Dirac gap $\sim 0.7 \text{ meV}$. The second one is a double VHS feature close to E_F at Γ point (highlighted by blue ellipses). Along $\Gamma - X$ direction they are electron

pockets centered at Γ and crossing E_F , while along $\Gamma - Y$ they are hole-like, yielding two saddle point VHSs.

When moving to $k_z = \pi$ plane ($Z - S - R - T - Z$ plane), the energy splitting between band pairs decreases and even vanishes, resulting in doubled band degeneracy. The DDC feature at X merges into a single, fourfold Dirac cone with a gapless, eightfold degenerate point at S (Fig. 2(h-i)). This eightfold fermion is symmetry-protected without SOC, determined by the projective irreducible representations (IReps) of the little group at S . Since the system is nonmagnetic without considering SOC, we only need to consider single-valued IReps. The nonsymmorphic group $Pmcn$ has higher dimension IReps at the boundary of the first BZ [61]. At S , the little group has two two-dimension IReps, which are conjugated to each other. Due to the time reversal symmetry, the two conjugated IReps will become a four-dimension IRep through the direct sum. Moreover, since the SOC here is negligible, the spin space has SU(2) symmetry protecting the spin degeneracy. Therefore, the band at the point S is eightfold degenerate. On the other hand, when considering SOC, the degeneracy will be determined by the double-valued projective IReps of the little group and the SU(2) symmetry will be broken. Although the double-valued IReps of the little group at S also include a four-dimension IRep, the time reversal cannot lead to eightfold degeneracy [16,20]. Therefore, SOC will generally open a gap at S . But the following ARPES measurement (unresolvable) and DFT analysis (~ 0.4 meV) both manifest that this SOC induced gap is negligible.

Besides, the double VHSs at Γ merge into one single VHS at Z , forming a fourfold VHS, robust against SOC. First, Z is invariant under inversion symmetry P and a glide mirror \tilde{M}_x : $(x, y, z) \rightarrow (-x, y + \frac{1}{2}, z + \frac{1}{2})$. In this case, if a Bloch state $|u\rangle$ is an eigenstate of \tilde{M}_x with eigenvalue g_x , there is another state of the system $P|u\rangle$. Moreover, because of the fractional translation of \tilde{M}_x , the two operators are anticommutative, $\{P, \tilde{M}_x\} = 0$, which gives $M_x P|u\rangle = -P\tilde{M}_x|u\rangle = -g_x P|u\rangle$. Thus, $|u\rangle$ and $P|u\rangle$ must be linearly independent for their opposite eigenvalues. Then, since Z is a time-reversal invariant momentum and the time reversal operator T has $T^2 = -1$, the band at this point has a Kramer double degeneracy. Therefore, for the states $|u\rangle$ and $P|u\rangle$, there must be linearly independent states $T|u\rangle$ and $TP|u\rangle$ having the same energy. Because $PT = TP$ here, $TP|u\rangle$ is equal to $PT|u\rangle$. So, the independence of $T|u\rangle$ and $TP|u\rangle$ can be also argued by the anticommutation relation. Furthermore, the Z point is also invariant under the combination of time reversal and inversion symmetries TP with $(TP)^2 = -1$. Thus, $TP|u\rangle$ is another Kramer-like double degenerate state of $|u\rangle$ at Z . Therefore, for any eigenstates $|u\rangle$ of \tilde{M}_x with momentum vector $(0, 0, \pi)$ in the crystal, there must be three linearly independent states $P|u\rangle, T|u\rangle$, and $TP|u\rangle$. Namely, the bands at Z are all fourfold degenerate.

Photon energy dependent ARPES measurement shown in Fig. 2(a) presents a periodic pattern of spectral intensity in the $k_x - k_z$ plane taken at $E_B = 0.13 \text{ eV}$, helping to define the high symmetry points of Γ, Z, X, S , using lattice constant $c = 17.78 \text{ \AA}$ and inner potential $V_0 = 13.5 \text{ eV}$. Fig. 2(e) shows the corresponding band dispersion along k_z direction at $k_x = 0.67 \text{ \AA}^{-1}$. Fermi surfaces mapped by ARPES at different k_z planes in Fig. 2(b) and 2(c) present features consistent with the DFT projection (Fig. 2(d)). Of particular interest are two elliptical features next to \bar{X} , which come from the DDC features along $\bar{\Gamma} - \bar{X} - \bar{\Gamma}$ direction. In Fig. 2(f-i), we compare the ARPES measured DDC spectra along $\Gamma - X - \Gamma$ and $Z - S - Z$ to the DFT calculated ones. For the DDC feature centered at X , the band pair splitting can be clearly resolved in the 2nd derivative plot and splitting bands are marked by yellow arrows shown in Fig. 2(f). It is noted that this splitting in ARPES spectra is more evident for the outer cones than the inner ones, probably resulting from the fact that the inner ones are more dispersed along k_z direction and its projection into the $k_x - k_y$ plane may smear out its own splitting. According to the above symmetry analysis, moving to $k_z = \pi$ plane merges the DDC feature into a single but fourfold degenerate Dirac cone, with an eightfold degenerate Dirac point (Fig. 2(i)). This is indeed observed in the ARPES spectral along $Z - S - Z$ direction as shown in Fig. 2(h). Compared to ARPES spectra along $\Gamma - X - \Gamma$, spectra along $Z - S - Z$ show the absence of band pair splitting and the presence of a degenerate point with enhanced spectral weight. These new features clearly prove the fourfold band degeneracy and the existence of eightfold fermion. The SOC induced gap ($\sim 0.4 \text{ meV}$ according to DFT in Fig. 2(i)) is negligible as compared to the breadth of observed bands in ARPES spectra (Fig. 2(h)).

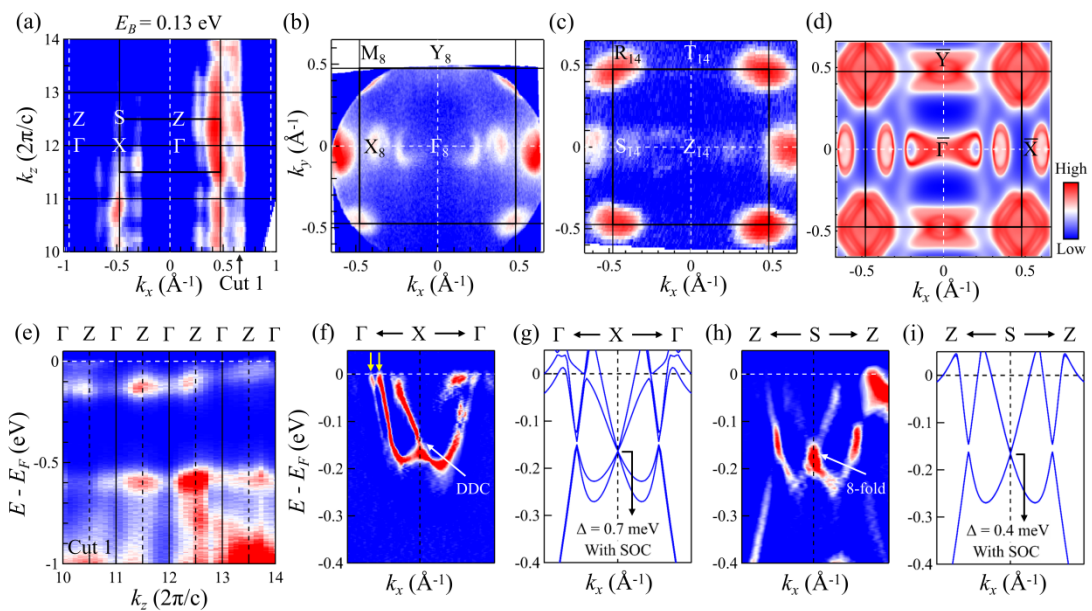


FIG. 2. Observation of practical eightfold fermions in TaCo₂Te₂. (a) Integrated photoemission intensity maps in the $k_x - k_z$ plane taken at $E_B = 0.13\text{ eV}$ measured by varying photon energy. (b, c) Fermi surface in the $k_x - k_y$ plane measured with photon energies 24 eV and 90 eV , respectively. (d) Fermi surface calculated by DFT with projection to the $k_x - k_y$ plane. (e) The band dispersion along the k_z direction at $k_x = 0.67\text{ \AA}^{-1}$ as shown in (a) Cut1. (f-i) ARPES measured spectra (2^{nd} derivative plot) and corresponding DFT calculated dispersions along high-symmetry paths with SOC.

We then focus on the fourfold VHS at the Z point as shown in Fig. 3(a). According to DFT, this VHS manifests itself as an electron pocket along $Z - S$ and a hole pocket along $Z - T$, thus as a saddle point with divergent density of states. To measure the corresponding spectra, we first align the $Z - S$ direction parallel to the measurement plane and then make a Fermi surface mapping. As shown by the mapping in Fig. 3(b), the spectral weight is heavily suppressed at Z in the first BZ due to the measurement geometry and orbital symmetry of the contributing electrons. So we choose the extended BZ to extract the cut along $S - Z - S$. As shown in Fig. 3(c), ARPES spectra indeed present an electron-like pocket centered at Z with its minimum binding energy $\sim 32\text{ meV}$. Then the sample is rotated by 90° so that $Z - T$ is parallel to the measurement plane. The ARPES spectra along $T - Z - T$ are extracted from the corresponding Fermi surface mapping (Fig. 3(d)). As shown in Fig. 3(e), a hole-like pocket centered at Z can be resolved. Comapring Fig. 3(c) and 3(e), it is found that the minimum of the electron pocket along $S - Z - S$ coincides with the maximum of the hole pocket along $T - Z - T$, being evidence of a saddle point. As our previous symmetry analysis has proved Z as a fourfold degenerate point, this saddle point is thus a fourfold degenerate VHS, which goes beyond the recent classifications of high order VHSs [56,57]. In the energy-resolved density of states (DOS) plot, a significant DOS enhancement at the saddle point energy can be seen (for details, see Fig. S1 [62]).

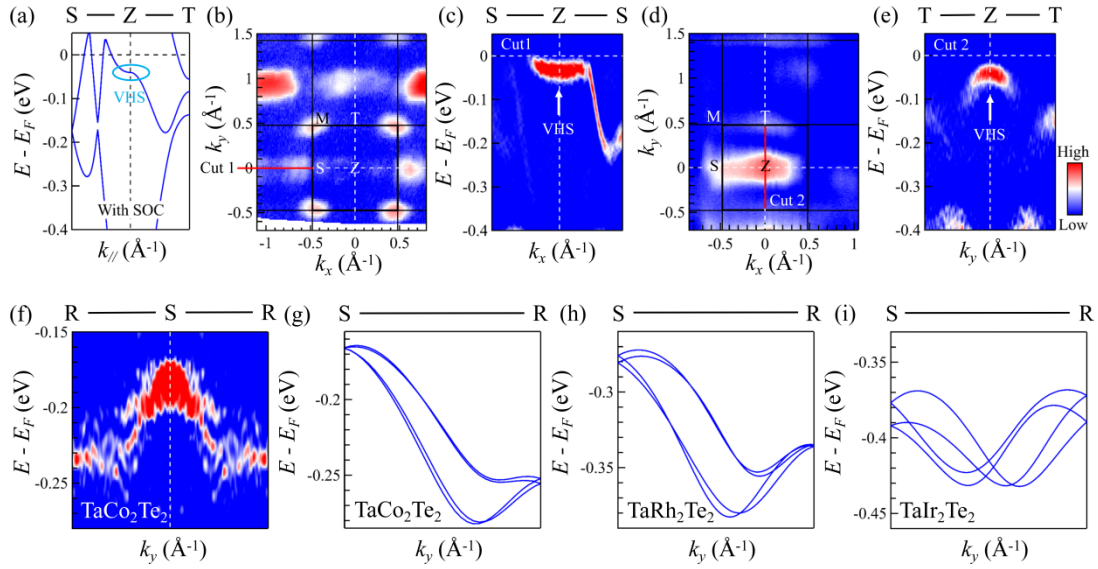


FIG. 3. Observation of fourfold VHSs in TaCo_2Te_2 and predicted realization of hourglass fermions in TaIr_2Te_2 . (a) DFT calculated fourfold bands along $S - Z - T$. (b, d) Fermi surface in $k_x - k_y$ plane measured with photon energy 90 eV, with the measurement plane defined by the incident light and emitted electrons parallel to $Z - S$ (b) and $Z - T$ (d) directions, respectively. (c, e) 2nd derivative ARPES spectra taken from the momentum cut indicated by red lines in (b) and (d), respectively. (f) 2nd derivative ARPES spectra showing the feature of hourglass fermion predicted in TaCo_2Te_2 . (g, h, i) DFT predicted hourglass fermions.

Discussion:

Combining magnetic, structural, electronic structure experiments and calculations, we have proved that TaCo_2Te_2 shows topological quantum critical behaviors related to its magnetic and electronic properties. Chemical substitution or applying strain may change the valence state of Co atoms and introduce large magnetic moments, so that long range magnetic order and magnetic quantum critical point are expected. The negligible SOC leads to the practical realization of eightfold fermions, which, according to theoretical analysis [16,20], serves as a topological quantum critical point. Symmetry breaking via magnetic field or uniaxial strain may lead to various topologically trivial or nontrivial phases such as Dirac point, Weyl point or nodal lines. The enhanced DOS by eightfold degeneracy and fourfold VHS also amplifies electron correlation, potentially resulting in various ordering instabilities and many-body interactions. Thus, we establish TaCo_2Te_2 as a conjoint topological and quantum critical platform with handful stimuli available to tune its physical properties.

We take SOC as an example of such a stimulus to theoretically demonstrate its tunability. As

shown in Fig. 3(g), the nonsymmorphic symmetry guarantees band features hosting hourglass fermions[18] along $S - R$ in TaCo_2Te_2 , distinct from surface hourglass fermions as discussed in KHgSb [63], which are the surface states in a type of topological insulators[18]. The bulk hourglass fermion in our work is a nodal loop semimetal constructed by the hourglass crossing points in the glide-invariant plane of the BZ [64,65]. It has been shown that the nodal loop in the bulk can give rise to drumhead surface states with a split band at the sample surface where the nodal loop is projected on [66]. As shown in Fig. 3(g), the predicted splitting between adjacent Dirac crossing is too small to be resolved in the ARPES spectra in Fig. 3(f). Increasing the effect of SOC, e.g., via substituting Co with Rh or Ir, would increase the adjacent Dirac crossing splitting and promote the practical observation of hourglass fermion features by ARPES. This expectation is indeed true as proved by our DFT calculation on the isostructural $\text{Ta}T_2\text{Te}_2$, where T represents Co, Rh, and Ir (Fig. S2). As shown in Fig. 3(g-i), in the considered energy-momentum region always exists an hourglass fermion feature for all the three materials. With increasing SOC, the energy splitting between adjacent Dirac points increases from $\sim 3 \text{ meV}$ in TaCo_2Te_2 to $\sim 15 \text{ meV}$ in TaIr_2Te_2 . The latter energy scale is comparable to the breadth of observed bands here, thus making the ARPES observation of hourglass fermions and the related drumhead surface states in TaIr_2Te_2 very promising. Our observation thus calls for further efforts to explore exotic states of matter and emergent phenomena intertwining magnetism, correlation, symmetry, and band topology based on the TaCo_2Te_2 family of materials.

ACKNOWLEDGEMENTS

This work is supported by the National Natural Science Foundation of China (NSFC) (Grants No. 12074163), Guangdong Basic and Applied Basic Research Foundation (Grants No. 2022B1515020046 and No. 2021B1515130007), the Guangdong Innovative and Entrepreneurial Research Team Program (Grants No. 2019ZT08C044), Shenzhen Science and Technology Program (Grant No. KQTD20190929173815000 and No. RCYX20200714114523069). C.C. acknowledges the assistance of SUSTech Core Research Facilities. The work at Beijing Institute of Technology was supported by the Natural Science Foundation of China (Grant No. 92065109), the National Key R&D Program of China (Grant No. 2020YFA0308800), the Beijing Natural Science Foundation (Grant No. Z190006, Z210006). Z.W. thanks the Analysis & Testing Center at BIT for assistance in facility support.

Materials and Methods

Sample growth and Characterizations

High quality TaCo_2Te_2 single crystals were synthesized by using a chemical vapor transport method with I_2 as a transport agent. The mixture of Ta powder (purity 99.9%), Co pieces (99.99%), and Te shot (99.99%) were prepared with a molar ratio of $\text{Ta} : \text{Co} : \text{Te} = 1 : 1 : 2$, and sealed in a quartz tube under high vacuum. Then it was placed in a horizon two-zone tube furnace and

maintained under a temperature gradient of 950 - 850 °C. After two weeks, shiny single crystals with a typical size of about $1 \times 2 \times 0.1$ mm³ were obtained. The structure of the crystals was characterized by x-ray diffraction with Cu $\text{K}\alpha$ radiation at room temperature using a Rigaku Miniex diffractometer. The diffraction pattern can be well indexed by the $(00l)$ reflections. Magnetic measurements were performed using the QD Magnetic Property Measurement System (MPMS) with the Vibrating Sample Magnetometer (VSM) mode. Temperature dependent magnetic susceptibility and the field-dependent magnetization results were collected with an external magnetic field of 0.2 T, which is parallel to the c axis.

ARPES measurement

ARPES measurements were performed at the beamline 13U of the National Synchrotron Radiation Laboratory (NSRL) and the beamline 1 of the Hiroshima Synchrotron Radiation Center (HSRC), Hiroshima, Japan. The energy resolution was set at 25 meV for Fermi surface mapping and 12.5meV for band structure measurements, respectively. The angular resolution was set at 0.1°. Samples were cleaved *in situ* along the (001) crystal plane under ultra-high vacuum with pressure better than 5×10^{-11} mbar and temperatures around 20 K.

First-principles calculations

The first-principles calculations are performed using the Vienna ab initio simulation package [67,68] within the projector augmented wave method [69]. The exchange correlation functional was treated within the generalized gradient approximation in the Perdew-Burke-Ernzerhof formalism [70]. The plane-wave basis with an energy cutoff of 500 eV. The BZ was sampled by using the Γ -centered $5 \times 5 \times 2$ Monkhorst-Pack grid [71] in the self-consistent calculation. The spin polarized calculations are calculated to give a nonmagnetic ground state. In addition, a tight-binding (TB) Hamiltonian based on the maximally localized Wannier functions (MLWF) [72] is constructed by using the Wannier90 package [73]. Through the TB Hamiltonian, the Fermi surface is further plotted by using the WannierTools package [74].

- [1] K. S. Novoselov, A. K. Geim, S. V. Morozov, D. Jiang, M. I. Katsnelson, I. V. Grigorieva, S. V. Dubonos & A. A. Firsov. Two-dimensional gas of massless Dirac fermions in graphene. *Nature* **438**, 197-200 (2005).
- [2] K. S. Novoselov, A. K. Geim, S. V. Morozov, D. Jiang, Y. Zhang, S. V. Dubonos, I. V. Grigorieva & A. A. Firsov. Electric Field Effect in Atomically Thin Carbon Films. *Science* **306**, 666-669, doi:10.1126/science.1102896 (2004).
- [3] D. Hsieh, D. Qian, L. Wray, Y. Xia, Y. S. Hor, R. J. Cava & M. Z. Hasan. A topological Dirac insulator in a quantum spin Hall phase. *Nature* **452**, 970-974 (2008).
- [4] Y. L. Chen, J. G. Analytis, J. H. Chu, Z. K. Liu, S. K. Mo, X. L. Qi, H. J. Zhang, D. H. Lu, X. Dai, Z. Fang, S. C. Zhang, I. R. Fisher, Z. Hussain & Z. X. Shen. Experimental Realization of a

- Three-Dimensional Topological Insulator, Bi₂Te₃. *Science* **325**, 178-181 (2009).
- [5] D. Hsieh, Y. Xia, D. Qian, L. Wray, J. H. Dil, F. Meier, J. Osterwalder, L. Patthey, J. G. Checkelsky, N. P. Ong, A. V. Fedorov, H. Lin, A. Bansil, D. Grauer, Y. S. Hor, R. J. Cava & M. Z. Hasan. A tunable topological insulator in the spin helical Dirac transport regime. *Nature* **460**, 1101-U1159 (2009).
- [6] Y. Xia, D. Qian, D. Hsieh, L. Wray, A. Pal, H. Lin, A. Bansil, D. Grauer, Y. S. Hor, R. J. Cava & M. Z. Hasan. Observation of a large-gap topological-insulator class with a single Dirac cone on the surface. *Nature Physics* **5**, 398-402 (2009).
- [7] B. Q. Lv, N. Xu, H. M. Weng, J. Z. Ma, P. Richard, X. C. Huang, L. X. Zhao, G. F. Chen, C. E. Matt, F. Bisti, V. N. Strocov, J. Mesot, Z. Fang, X. Dai, T. Qian, M. Shi & H. Ding. Observation of Weyl nodes in TaAs. *Nature Physics* **11**, 724-727, doi:10.1038/nphys3426 (2015).
- [8] Su-Yang Xu, Nasser Alidoust, Ilya Belopolski, Zhujun Yuan, Guang Bian, Tay-Rong Chang, Hao Zheng, Vladimir N. Strocov, Daniel S. Sanchez, Guoqing Chang, Chenglong Zhang, Daixiang Mou, Yun Wu, Lunan Huang, Chi-Cheng Lee, Shin-Ming Huang, BaoKai Wang, Arun Bansil, Horng-Tay Jeng, Titus Neupert, Adam Kaminski, Hsin Lin, Shuang Jia & M. Zahid Hasan. Discovery of a Weyl fermion state with Fermi arcs in niobium arsenide. *Nature Physics* **11**, 748-754, doi:10.1038/nphys3437 (2015).
- [9] Su-Yang Xu, Ilya Belopolski, Nasser Alidoust, Madhab Neupane, Guang Bian, Chenglong Zhang, Raman Sankar, Guoqing Chang, Zhujun Yuan, Chi-Cheng Lee, Shin-Ming Huang, Hao Zheng, Jie Ma, Daniel S. Sanchez, BaoKai Wang, Arun Bansil, Fangcheng Chou, Pavel P. Shibayev, Hsin Lin, Shuang Jia & M. Zahid Hasan. Discovery of a Weyl fermion semimetal and topological Fermi arcs. *Science* **349**, 613 (2015).
- [10] Su-Yang Xu, Chang Liu, Satya K. Kushwaha, Raman Sankar, Jason W. Krizan, Ilya Belopolski, Madhab Neupane, Guang Bian, Nasser Alidoust, Tay-Rong Chang, Horng-Tay Jeng, Cheng-Yi Huang, Wei-Feng Tsai, Hsin Lin, Pavel P. Shibayev, Fang-Cheng Chou, Robert J. Cava & M. Zahid Hasan. Observation of Fermi arc surface states in a topological metal. *Science* **347**, 294 (2015).
- [11] L. X. Yang, Z. K. Liu, Y. Sun, H. Peng, H. F. Yang, T. Zhang, B. Zhou, Y. Zhang, Y. F. Guo, M. Rahn, D. Prabhakaran, Z. Hussain, S. K. Mo, C. Felser, B. Yan & Y. L. Chen. Weyl semimetal phase in the non-centrosymmetric compound TaAs. *Nature Physics* **11**, 728-732, doi:10.1038/nphys3425 (2015).
- [12] Z. K. Liu, J. Jiang, B. Zhou, Z. J. Wang, Y. Zhang, H. M. Weng, D. Prabhakaran, S. K. Mo, H. Peng, P. Dudin, T. Kim, M. Hoesch, Z. Fang, X. Dai, Z. X. Shen, D. L. Feng, Z. Hussain & Y. L. Chen. A stable three-dimensional topological Dirac semimetal Cd₃As₂. *Nat Mater* **13**, 677-681, doi:10.1038/nmat3990 (2014).
- [13] Z. K. Liu, B. Zhou, Y. Zhang, Z. J. Wang, H. M. Weng, D. Prabhakaran, S. K. Mo, Z. X. Shen, Z. Fang, X. Dai, Z. Hussain & Y. L. Chen. Discovery of a Three-Dimensional Topological Dirac Semimetal, Na₃Bi. *Science* **343**, 864 (2014).
- [14] Su-Yang Xu, Chang Liu, Satya K. Kushwaha, Raman Sankar, Jason W. Krizan, Ilya Belopolski, Madhab Neupane, Guang Bian, Nasser Alidoust, Tay-Rong Chang, Horng-Tay Jeng, Cheng-Yi Huang, Wei-Feng Tsai, Hsin Lin, Pavel P. Shibayev, Fang-Cheng Chou, Robert J. Cava & M. Zahid Hasan. Observation of Fermi arc surface states in a topological metal. *Science* **347**, 294-298, doi:doi:10.1126/science.1256742

- (2015).
- [15] A. Alexandradinata, Zhijun Wang & B. Andrei Bernevig. Topological Insulators from Group Cohomology. *Physical Review X* **6**, doi:10.1103/PhysRevX.6.021008 (2016).
- [16] B. Bradlyn, J. Cano, Z. Wang, M. G. Vergniory, C. Felser, R. J. Cava & B. A. Bernevig. Beyond Dirac and Weyl fermions: Unconventional quasiparticles in conventional crystals. *Science* **353**, aaf5037, doi:10.1126/science.aaf5037 (2016).
- [17] S. M. Huang, S. Y. Xu, I. Belopolski, C. C. Lee, G. Chang, T. R. Chang, B. Wang, N. Alidoust, G. Bian, M. Neupane, D. Sanchez, H. Zheng, H. T. Jeng, A. Bansil, T. Neupert, H. Lin & M. Z. Hasan. New type of Weyl semimetal with quadratic double Weyl fermions. *Proc Natl Acad Sci U S A* **113**, 1180-1185, doi:10.1073/pnas.1514581113 (2016).
- [18] Z. Wang, A. Alexandradinata, R. J. Cava & B. A. Bernevig. Hourglass fermions. *Nature* **532**, 189-194, doi:10.1038/nature17410 (2016).
- [19] Hongming Weng, Chen Fang, Zhong Fang & Xi Dai. Topological semimetals with triply degenerate nodal points in θ -phase tantalum nitride. *Physical Review B* **93**, doi:10.1103/PhysRevB.93.241202 (2016).
- [20] B. J. Wieder, Y. Kim, A. M. Rappe & C. L. Kane. Double Dirac Semimetals in Three Dimensions. *Phys Rev Lett* **116**, 186402, doi:10.1103/PhysRevLett.116.186402 (2016).
- [21] Ziming Zhu, Georg W. Winkler, QuanSheng Wu, Ju Li & Alexey A. Soluyanov. Triple Point Topological Metals. *Physical Review X* **6**, doi:10.1103/PhysRevX.6.031003 (2016).
- [22] Qihang Liu & Alex Zunger. Predicted Realization of Cubic Dirac Fermion in Quasi-One-Dimensional Transition-Metal Monochalcogenides. *Physical Review X* **7**, doi:10.1103/PhysRevX.7.021019 (2017).
- [23] Benjamin J. Wieder, Barry Bradlyn, Zhijun Wang, Jennifer Cano, Youngkuk Kim, Hyeong-Seok D. Kim, Andrew M. Rappe, C. L. Kane & B. Andrei Bernevig. Wallpaper fermions and the nonsymmorphic Dirac insulator. *Science* **361**, 246, doi:10.1126/science.aan2802 (2018).
- [24] Weikang Wu, Zhi-Ming Yu, Xiaoting Zhou, Y. X. Zhao & Shengyuan A. Yang. Higher-order Dirac fermions in three dimensions. *Physical Review B* **101**, doi:10.1103/PhysRevB.101.205134 (2020).
- [25] P. J. Guo, Y. W. Wei, K. Liu, Z. X. Liu & Z. Y. Lu. Eightfold Degenerate Fermions in Two Dimensions. *Phys Rev Lett* **127**, 176401, doi:10.1103/PhysRevLett.127.176401 (2021).
- [26] Jennifer Cano, Barry Bradlyn & M. G. Vergniory. Multifold nodal points in magnetic materials. *APL Materials* **7**, doi:10.1063/1.5124314 (2019).
- [27] Ke Deng, Guoliang Wan, Peng Deng, Kenan Zhang, Shijie Ding, Eryin Wang, Mingzhe Yan, Huaqing Huang, Hongyun Zhang, Zhilin Xu, Jonathan Denlinger, Alexei Fedorov, Haitao Yang, Wenhui Duan, Hong Yao, Yang Wu, Shoushan Fan, Haijun Zhang, Xi Chen & Shuyun Zhou. Experimental observation of topological Fermi arcs in type-II Weyl semimetal MoTe₂. *Nature Physics* **12**, 1105-1110, doi:10.1038/nphys3871 (2016).
- [28] L. Huang, T. M. McCormick, M. Ochi, Z. Zhao, M. T. Suzuki, R. Arita, Y. Wu, D. Mou, H. Cao, J. Yan, N. Trivedi & A. Kaminski. Spectroscopic evidence for a type II Weyl semimetallic state in MoTe₂. *Nat Mater* **15**, 1155-1160, doi:10.1038/nmat4685 (2016).
- [29] J. Jiang, Z. K. Liu, Y. Sun, H. F. Yang, C. R. Rajamathi, Y. P. Qi, L. X. Yang, C. Chen, H. Peng, C. C. Hwang, S. Z. Sun, S. K. Mo, I. Vobornik, J. Fujii, S. S. Parkin, C. Felser, B. H. Yan & Y. L. Chen. Signature of type-II Weyl semimetal phase in MoTe₂. *Nat Commun* **8**, 13973,

- doi:10.1038/ncomms13973 (2017).
- [30] Su-Yang Xu, Nasser Alidoust, Guoqing Chang, Hong Lu, Bahadur Singh, Ilya Belopolski, Daniel S. Sanchez, Xiao Zhang, Guang Bian, Hao Zheng, Marius-Adrian Husanu, Yi Bian, Shin-Ming Huang, Chuang-Han Hsu, Tay-Rong Chang, Horng-Tay Jeng, Arun Bansil, Titus Neupert, Vladimir N. Strocov, Hsin Lin, Shuang Jia & M. Zahid Hasan. Discovery of Lorentz-violating type II Weyl fermions in LaAlGe. *Science Advances* **3**, e1603266, doi:doi:10.1126/sciadv.1603266 (2017).
- [31] I. Belopolski, P. Yu, D. S. Sanchez, Y. Ishida, T. R. Chang, S. S. Zhang, S. Y. Xu, H. Zheng, G. Chang, G. Bian, H. T. Jeng, T. Kondo, H. Lin, Z. Liu, S. Shin & M. Z. Hasan. Signatures of a time-reversal symmetric Weyl semimetal with only four Weyl points. *Nat Commun* **8**, 942, doi:10.1038/s41467-017-00938-1 (2017).
- [32] S. Borisenko, D. Evtushinsky, Q. Gibson, A. Yaresko, K. Koepernik, T. Kim, M. Ali, J. van den Brink, M. Hoesch, A. Fedorov, E. Haubold, Y. Kushnirenko, I. Soldatov, R. Schafer & R. J. Cava. Time-reversal symmetry breaking type-II Weyl state in YbMnBi₂. *Nat Commun* **10**, 3424, doi:10.1038/s41467-019-11393-5 (2019).
- [33] Ilya Belopolski, Kaustuv Manna, Daniel S. Sanchez, Guoqing Chang, Benedikt Ernst, Jiaxin Yin, Songtian S. Zhang, Tyler Cochran, Nana Shumiya, Hao Zheng, Bahadur Singh, Guang Bian, Daniel Multer, Maksim Litskevich, Xiaoting Zhou, Shin-Ming Huang, Baokai Wang, Tay-Rong Chang, Su-Yang Xu, Arun Bansil, Claudia Felser, Hsin Lin & M. Zahid Hasan. Discovery of topological Weyl fermion lines and drumhead surface states in a room temperature magnet. *Science* **365**, 1278, doi:10.1126/science.aav2327 (2019).
- [34] D. F. Liu, A. J. Liang, E. K. Liu, Q. N. Xu, Y. W. Li, C. Chen, D. Pei, W. J. Shi, S. K. Mo, P. Dudin, T. Kim, C. Cacho, G. Li, Y. Sun, L. X. Yang, Z. K. Liu, S. S. P. Parkin, C. Felser & Y. L. Chen. Magnetic Weyl semimetal phase in a Kagomé crystal. *Science* **365**, 1282, doi:10.1126/science.aav2873 (2019).
- [35] B. Q. Lv, Z. L. Feng, Q. N. Xu, X. Gao, J. Z. Ma, L. Y. Kong, P. Richard, Y. B. Huang, V. N. Strocov, C. Fang, H. M. Weng, Y. G. Shi, T. Qian & H. Ding. Observation of three-component fermions in the topological semimetal molybdenum phosphide. *Nature* **546**, 627–631, doi:10.1038/nature22390 (2017).
- [36] J. Z. Ma, J. B. He, Y. F. Xu, B. Q. Lv, D. Chen, W. L. Zhu, S. Zhang, L. Y. Kong, X. Gao, L. Y. Rong, Y. B. Huang, P. Richard, C. Y. Xi, E. S. Choi, Y. Shao, Y. L. Wang, H. J. Gao, X. Dai, C. Fang, H. M. Weng, G. F. Chen, T. Qian & H. Ding. Three-component fermions with surface Fermi arcs in tungsten carbide. *Nature Physics* **14**, 349–354, doi:10.1038/s41567-017-0021-8 (2018).
- [37] Yiwei Li, Yunyouyou Xia, Sandy Adhitia Ekahana, Nitesh Kumar, Juan Jiang, Lexian Yang, Cheng Chen, Chaoxing Liu, Binghai Yan, Claudia Felser, Gang Li, Zhongkai Liu & Yulin Chen. Topological origin of the type-II Dirac fermions in PtSe₂. *Physical Review Materials* **1**, doi:10.1103/PhysRevMaterials.1.074202 (2017).
- [38] Kenan Zhang, Mingzhe Yan, Haoxiong Zhang, Huajing Huang, Masashi Arita, Zhe Sun, Wenhui Duan, Yang Wu & Shuyun Zhou. Experimental evidence for type-II Dirac semimetal in PtSe₂. *Physical Review B* **96**, doi:10.1103/PhysRevB.96.125102 (2017).
- [39] M. S. Bahramy, O. J. Clark, B. J. Yang, J. Feng, L. Bawden, J. M. Riley, I. Markovic, F. Mazzola, V. Sunko, D. Biswas, S. P. Cooil, M. Jorge, J. W. Wells, M. Leandersson, T. Balasubramanian, J. Fujii, I. Vobornik, J. E. Rault, T. K. Kim, M. Hoesch, K. Okawa, M.

- Asakawa, T. Sasagawa, T. Eknapakul, W. Meevasana & P. D. C. King. Ubiquitous formation of bulk Dirac cones and topological surface states from a single orbital manifold in transition-metal dichalcogenides. *Nat Mater* **17**, 21–28, doi:10.1038/nmat5031 (2018).
- [40] Fucong Fei, Xiangyan Bo, Rui Wang, Bin Wu, Juan Jiang, Dongzhi Fu, Ming Gao, Hao Zheng, Yulin Chen, Xuefeng Wang, Haijun Bu, Fengqi Song, Xiangang Wan, Baigeng Wang & Guanghou Wang. Nontrivial Berry phase and type-II Dirac transport in the layered material PdTe₂. *Physical Review B* **96**, doi:10.1103/PhysRevB.96.041201 (2017).
- [41] H. J. Noh, J. Jeong, E. J. Cho, K. Kim, B. I. Min & B. G. Park. Experimental Realization of Type-II Dirac Fermions in a PdTe_{2} Superconductor. *Phys Rev Lett* **119**, 016401, doi:10.1103/PhysRevLett.119.016401 (2017).
- [42] M. Yan, H. Huang, K. Zhang, E. Wang, W. Yao, K. Deng, G. Wan, H. Zhang, M. Arita, H. Yang, Z. Sun, H. Yao, Y. Wu, S. Fan, W. Duan & S. Zhou. Lorentz-violating type-II Dirac fermions in transition metal dichalcogenide PtTe₂. *Nat Commun* **8**, 257, doi:10.1038/s41467-017-00280-6 (2017).
- [43] H. Miao, T. T. Zhang, L. Wang, D. Meyers, A. H. Said, Y. L. Wang, Y. G. Shi, H. M. Weng, Z. Fang & M. P. M. Dean. Observation of Double Weyl Phonons in Parity-Breaking FeSi. *Phys Rev Lett* **121**, 035302, doi:10.1103/PhysRevLett.121.035302 (2018).
- [44] Z. Rao, H. Li, T. Zhang, S. Tian, C. Li, B. Fu, C. Tang, L. Wang, Z. Li, W. Fan, J. Li, Y. Huang, Z. Liu, Y. Long, C. Fang, H. Weng, Y. Shi, H. Lei, Y. Sun, T. Qian & H. Ding. Observation of unconventional chiral fermions with long Fermi arcs in CoSi. *Nature* **567**, 496–499, doi:10.1038/s41586-019-1031-8 (2019).
- [45] D. S. Sanchez, I. Belopolski, T. A. Cochran, X. Xu, J. X. Yin, G. Chang, W. Xie, K. Manna, V. Suss, C. Y. Huang, N. Alidoust, D. Multer, S. S. Zhang, N. Shumiya, X. Wang, G. Q. Wang, T. R. Chang, C. Felser, S. Y. Xu, S. Jia, H. Lin & M. Z. Hasan. Topological chiral crystals with helicoid-arc quantum states. *Nature* **567**, 500–505, doi:10.1038/s41586-019-1037-2 (2019).
- [46] Niels B. M. Schröter, Ding Pei, Maia G. Vergniory, Yan Sun, Kaustuv Manna, Fernando de Juan, Jonas A. Krieger, Vicky Süss, Marcus Schmidt, Pavel Dudin, Barry Bradlyn, Timur K. Kim, Thorsten Schmitt, Cephise Cacho, Claudia Felser, Vladimir N. Strocov & Yulin Chen. Chiral topological semimetal with multifold band crossings and long Fermi arcs. *Nature Physics* **15**, 759–765, doi:10.1038/s41567-019-0511-y (2019).
- [47] D. Takane, Z. Wang, S. Souma, K. Nakayama, T. Nakamura, H. Oinuma, Y. Nakata, H. Iwasawa, C. Cacho, T. Kim, K. Horiba, H. Kumigashira, T. Takahashi, Y. Ando & T. Sato. Observation of Chiral Fermions with a Large Topological Charge and Associated Fermi-Arc Surface States in CoSi. *Phys Rev Lett* **122**, 076402, doi:10.1103/PhysRevLett.122.076402 (2019).
- [48] B. Q. Lv, Z. L. Feng, J. Z. Zhao, Noah F. Q. Yuan, A. Zong, K. F. Luo, R. Yu, Y. B. Huang, V. N. Strocov, A. Chikina, A. A. Soluyanov, N. Gedik, Y. G. Shi, T. Qian & H. Ding. Observation of multiple types of topological fermions in PdBiSe. *Physical Review B* **99**, doi:10.1103/PhysRevB.99.241104 (2019).
- [49] C. Z. Xu, Y. H. Chan, Y. Chen, P. Chen, X. Wang, C. Dejoie, M. H. Wong, J. A. Hlevyack, H. Ryu, H. Y. Kee, N. Tamura, M. Y. Chou, Z. Hussain, S. K. Mo & T. C. Chiang. Elemental Topological Dirac Semimetal: alpha-Sn on InSb(111). *Phys Rev Lett* **118**, 146402, doi:10.1103/PhysRevLett.118.146402 (2017).

- [50] N. Kumar, M. Yao, J. Nayak, M. G. Vergniory, J. Bannies, Z. Wang, N. B. M. Schroter, V. N. Strocov, L. Muchler, W. Shi, E. D. L. Rienks, J. L. Manes, C. Shekhar, S. S. P. Parkin, J. Fink, G. H. Fecher, Y. Sun, B. A. Bernevig & C. Felser. Signatures of Sixfold Degenerate Exotic Fermions in a Superconducting Metal PdSb₂. *Adv Mater* **32**, e1906046, doi:10.1002/adma.201906046 (2020).
- [51] Z. P. Sun, C. Q. Hua, X. L. Liu, Z. T. Liu, M. Ye, S. Qiao, Z. H. Liu, J. S. Liu, Y. F. Guo, Y. H. Lu & D. W. Shen. Direct observation of sixfold exotic fermions in the pyrite-structured topological semimetal PdSb₂. *Physical Review B* **101**, doi:10.1103/PhysRevB.101.155114 (2020).
- [52] Xiàn Yáng, Tyler A. Cochran, Ramakanta Chapai, Damien Tristant, Jia-Xin Yin, Ilya Belopolski, Zījiā Chéng, Daniel Multer, Songtian S. Zhang, Nana Shumiya, Maksim Litskevich, Yuxiao Jiang, Guoqing Chang, Qi Zhang, Ilya Vekhter, William A. Shelton, Rongying Jin, Su-Yang Xu & M. Zahid Hasan. Observation of sixfold degenerate fermions in PdSb₂. *Physical Review B* **101**, doi:10.1103/PhysRevB.101.201105 (2020).
- [53] R. Chapai, A. Rydh, M. P. Smylie, D. Y. Chung, H. Zheng, A. E. Koshelev, J. E. Pearson, W. K. Kwok, J. F. Mitchell & U. Welp. Superconducting properties of the spin Hall candidate Ta₃Sb with eightfold degeneracy. *Physical Review B* **105**, doi:10.1103/PhysRevB.105.184510 (2022).
- [54] Xi Zhang, Qiangqiang Gu, Haigen Sun, Tianchuang Luo, Yanzhao Liu, Yueyuan Chen, Zhibin Shao, Zongyuan Zhang, Shaojian Li, Yuanwei Sun, Yuehui Li, Xiaokang Li, Shangjie Xue, Jun Ge, Ying Xing, R. Comin, Zengwei Zhu, Peng Gao, Binghai Yan, Ji Feng, Minghu Pan & Jian Wang. Eightfold fermionic excitation in a charge density wave compound. *Physical Review B* **102**, doi:10.1103/PhysRevB.102.035125 (2020).
- [55] Tanya Berry, Lucas A. Pressley, W. Adam Phelan, Thao T. Tran & Tyrel M. McQueen. Laser-Enhanced Single Crystal Growth of Non-Symmorphic Materials: Applications to an Eight-Fold Fermion Candidate. *Chemistry of Materials* **32**, 5827-5834, doi:10.1021/acs.chemmater.0c01721 (2020).
- [56] N. F. Q. Yuan, H. Isobe & L. Fu. Magic of high-order van Hove singularity. *Nat Commun* **10**, 5769, doi:10.1038/s41467-019-13670-9 (2019).
- [57] Noah F. Q. Yuan & Liang Fu. Classification of critical points in energy bands based on topology, scaling, and symmetry. *Physical Review B* **101**, doi:10.1103/PhysRevB.101.125120 (2020).
- [58] Ratnadwip Singha, Fang Yuan, Guangming Cheng, Tyger H. Salters, Yuzki M. Oey, Graciela V. Villalpando, Milena Jovanovic, Nan Yao & Leslie M. Schoop. TaCo₂Te₂ : An Air-Stable, High Mobility Van der Waals Material with Probable Magnetic Order. *Advanced Functional Materials* **32**, doi:10.1002/adfm.202108920 (2021).
- [59] Q. Wang, Y. Xu, R. Lou, Z. Liu, M. Li, Y. Huang, D. Shen, H. Weng, S. Wang & H. Lei. Large intrinsic anomalous Hall effect in half-metallic ferromagnet Co₃Sn₂S₂ with magnetic Weyl fermions. *Nat Commun* **9**, 3681, doi:10.1038/s41467-018-06088-2 (2018).
- [60] E. Liu, Y. Sun, N. Kumar, L. Muchler, A. Sun, L. Jiao, S. Y. Yang, D. Liu, A. Liang, Q. Xu, J. Kroder, V. Suss, H. Borrmann, C. Shekhar, Z. Wang, C. Xi, W. Wang, W. Schnelle, S. Wirth, Y. Chen, S. T. B. Goennenwein & C. Felser. Giant anomalous Hall effect in a ferromagnetic Kagome-lattice semimetal. *Nat Phys* **14**, 1125-1131, doi:10.1038/s41567-018-0234-5 (2018).

- [61] www.cryst.ehu.es
- [62] See supplementary
- [63] Junzhang Ma, Changjiang Yi, Baiqing Lv, ZhiJun Wang, Simin Nie, Le Wang, Lingyuan Kong, Yaobo Huang, Pierre Richard, Peng Zhang, Koichiro Yaji, Kenta Kuroda, Shik Shin, Hongming Weng, Bogdan Andrei Bernevig, Youguo Shi, Tian Qian & Hong Ding. Experimental evidence of hourglass fermion in the candidate nonsymmorphic topological insulator KHgSb. *Science Advances* **3**, e1602415, doi:10.1126/sciadv.1602415 (2017).
- [64] Luyang Wang, Shao-Kai Jian & Hong Yao. Hourglass semimetals with nonsymmorphic symmetries in three dimensions. *Physical Review B* **96**, doi:10.1103/PhysRevB.96.075110 (2017).
- [65] Si Li, Ying Liu, Shan-Shan Wang, Zhi-Ming Yu, Shan Guan, Xian-Lei Sheng, Yugui Yao & Shengyuan A. Yang. Nonsymmorphic-symmetry-protected hourglass Dirac loop, nodal line, and Dirac point in bulk and monolayer X₃SiTe₆ (X = Ta, Nb). *Physical Review B* **97**, doi:10.1103/PhysRevB.97.045131 (2018).
- [66] Hongming Weng, Yunye Liang, Qiunan Xu, Rui Yu, Zhong Fang, Xi Dai & Yoshiyuki Kawazoe. Topological node-line semimetal in three-dimensional graphene networks. *Physical Review B* **92**, doi:10.1103/PhysRevB.92.045108 (2015).
- [67] G. Kresse & J. Furthmüller. Efficient iterative schemes for ab initio total-energy calculations using a plane-wave basis set. *Physical Review B* **54**, 11169-11186, doi:10.1103/PhysRevB.54.11169 (1996).
- [68] G. Kresse & D. Joubert. From ultrasoft pseudopotentials to the projector augmented-wave method. *Physical Review B* **59**, 1758-1775, doi:10.1103/PhysRevB.59.1758 (1999).
- [69] P. E. Blöchl. Projector augmented-wave method. *Physical Review B* **50**, 17953-17979, doi:10.1103/PhysRevB.50.17953 (1994).
- [70] John P. Perdew, Kieron Burke & Matthias Ernzerhof. Generalized Gradient Approximation Made Simple. *Physical Review Letters* **77**, 3865-3868, doi:10.1103/PhysRevLett.77.3865 (1996).
- [71] Hendrik J. Monkhorst & James D. Pack. Special points for Brillouin-zone integrations. *Physical Review B* **13**, 5188-5192, doi:10.1103/PhysRevB.13.5188 (1976).
- [72] Ivo Souza, Nicola Marzari & David Vanderbilt. Maximally localized Wannier functions for entangled energy bands. *Physical Review B* **65**, 035109, doi:10.1103/PhysRevB.65.035109 (2001).
- [73] Giovanni Pizzi, Valerio Vitale, Ryotaro Arita, Stefan Blügel, Frank Freimuth, Guillaume Géranton, Marco Gibertini, Dominik Gresch, Charles Johnson, Takashi Koretsune, Julen Ibañez-Azpiroz, Hyungjun Lee, Jae-Mo Lihm, Daniel Marchand, Antimo Marrazzo, Yuriy Mokrousov, Jamal I. Mustafa, Yoshiro Nohara, Yusuke Nomura, Lorenzo Paulatto, Samuel Poncé, Thomas Ponweiser, Junfeng Qiao, Florian Thöle, Stepan S. Tsirkin, Małgorzata Wierzbowska, Nicola Marzari, David Vanderbilt, Ivo Souza, Arash A. Mostofi & Jonathan R. Yates. Wannier90 as a community code: new features and applications. *Journal of Physics: Condensed Matter* **32**, 165902, doi:10.1088/1361-648x/ab51ff (2020).
- [74] QuanSheng Wu, ShengNan Zhang, Hai-Feng Song, Matthias Troyer & Alexey A. Soluyanov. WannierTools: An open-source software package for novel topological

materials. *Computer Physics Communications* **224**, 405-416,
doi:<https://doi.org/10.1016/j.cpc.2017.09.033> (2018).